HYDRODYNAMIC MODELLING OF MODULARIZED FLOATING PHOTOVOLTAICS ARRAYS

De-Qing Zhang
College of Engineering, Ocean University of China, Qingdao, China

Jun-Feng Du
College of Engineering, Ocean University of China, Qingdao, China

Zhi-Ming Yuan
Department of Naval Architecture, Ocean & Engineering, University of Strathclyde, Glasgow, UK

Ming Zhang
Department of Naval Architecture, Ocean & Engineering, University of Strathclyde, Glasgow, UK

Feng-Shen Zhu
Department of Naval Architecture, Ocean & Engineering, University of Strathclyde, Glasgow, UK

ABSTRACT

Large arrays of floating photovoltaics (FPV) are emerging to be an attractive solution to renewable energy production and ocean space utilization. FPV arrays are typically buoyed by hundreds of modularized floating bases arranged in ocean surface. The total performance of the FPV arrays is significantly affected by the hydrodynamic interactions between these individual floaters. As the size of the array increases, more time will be required to calculate the entire hydrodynamic properties. From the engineering point of view, it is a challenging task to fully consider the radiation interactions among the modularized FPV floaters. In fact, when the distance between two floating bodies is large enough, their interaction will gradually vanish. The present study developed a cut-off scheme to improve the computational efficiency while providing a reliable prediction of the interaction effects in engineering practice. A cut-off radius is introduced in this scheme to determine the coupling range in which the radiation hydrodynamic interactions should be considered. The cut-off radius is determined by three parameters, including the modular shape, wave frequency and accuracy requirement. Several arrays of rectangular FPV bases were taken as examples to show how to quantify the radiation interactions and find an optimal cut-off radius. The effect of wave direction, gap distance, and connection type were also investigated. The results from the validation case showed that the hydrodynamic interaction can be well predicted using the proposed cut-off scheme, while more than half of the computational time can be saved.

Keywords: FPV array, modularized floating structures, radiation interaction, cut-off radius, linear potential flow

1. INTRODUCTION

With the increase in energy consumption, the depletion of fossil fuels, and the emission of greenhouse gas, there is an increasing interest to develop renewable and carbon-emission-free energies. Floating photovoltaic (FPV) arrays have been considered to be one of the most promising power generation systems [1]. Compared to land-based solar panel plants, solar FPV systems offer a number of significant advantages, such as fewer barriers to sunlight, savings in scarce land resources, and higher power generation efficiency due to the lower temperatures beneath the panels [2,3]. In addition, solar FPV arrays are often combined with other renewable energy plants to form a hybrid power production system [4]. Figure 1 shows a sketch of an FPV array combined with a fixed wind turbine farm. For FPV arrays, the solar panels are buoyed by hundreds of floaters deployed in the same geographic location and arranged systematically on the ocean surface. However, it is a challenging issue to fully consider the hydrodynamic interactions among these floaters in an FPV array. Hydrodynamic modelling of modularized floating photovoltaics arrays

Most of the published works mainly focused on the prediction of the hydrodynamic interaction effects between two or three bodies. Zheng and Zhang [5] carried out a frequency-domain analysis to evaluate the wave power capture capacity of two interconnected floats with arbitrary lengths. Liang [6] investigated the fluid resonance in a gap between two side-by-side vessels. Jin [7] employed a two-body model to predict the annual power generation of a hinged raft wave energy converter (WEC). Due to the increasing complexity and computational

This is a peer-reviewed, version of record of the following paper: Zhang, D-Q., Du, J-F., Yuan, Z-M., Zhang, M., & Zhu, F-S. (in press). Hydrodynamic modelling of modularized floating photovoltaics arrays. In Proceedings of the ASME 2023 42st International Conference on Ocean, Offshore and Arctic Engineering Article 102530 ASME.

cost of large numbers of interacting floaters, studies on large-scale devices are relatively rare. Borgarino [8] used a boundary element method to investigate the effect of the separating distance between 9-25 heaving cylinders and surging barges. Their results clearly showed that the diffracted and radiated waves led to a sufficient increase in energy absorption. Engström [9] assessed the smoothing effect of an array of 32 point-absorbing WECs. The results showed that the variance in power production depends crucially on the geometry of the array and the number of interacting devices.

To save the computational resources when modelling the hydrodynamic properties of large arrays of interacting bodies, fast algorithms are designed to accelerate the simulations, including the fast multipole method [10,11] and pre-corrected fast Fourier transforms [12]. In addition, some simplified methods are also proposed [13-15]. However, these approaches have many limitations in the applications [16].

In the present study, an interaction cut-off scheme, which can be implemented in the multi-body hydrodynamic solvers, is proposed to model the hydrodynamic properties of large arrays of modularized FPV floaters. The proposed scheme makes it feasible to quickly determine the scope outside which the radiation hydrodynamic interactions can be ignored in the calculations. The results from a series of 8-floater FPV array cases show that the motion responses can be well predicted by the present cut-off scheme. The effect of wave direction, gap distance, and connection type are also investigated.

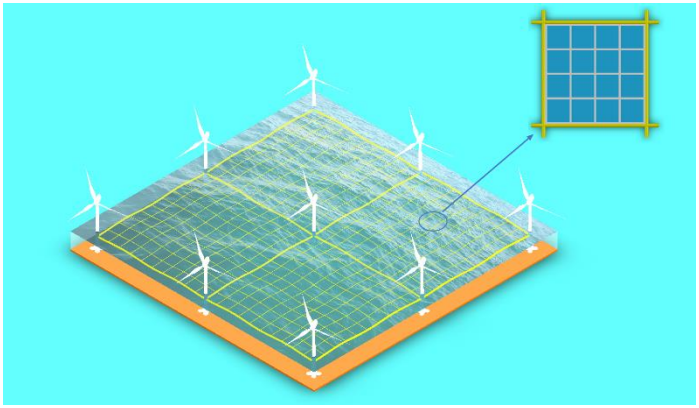

FIGURE 1: AN FPV ARRAY COMBINED WITH THE WIND TURBINES FARM.

2. NUMERICAL MODELLING METHODS

2.1 Mathematical formulations of the potentials

Considering the *N*-body array oscillating in the open sea, the corresponding right-handed coordinate systems are presented in Figure 2. The global coordinate system *O-XYZ* is defined on the undisturbed free surface, and the body coordinate systems o_m-$x_m y_m z_m$ (m=1, 2, …, N) are fixed at midships of each floater with the body coordinate origins locating on the mean free surface. The incident wave direction is defined as the angle between the wave propagation direction and *X*-axis. In the computation, the motions and forces are transferred to the local coordinate system in which the origin is placed at the centre of gravity of each body.

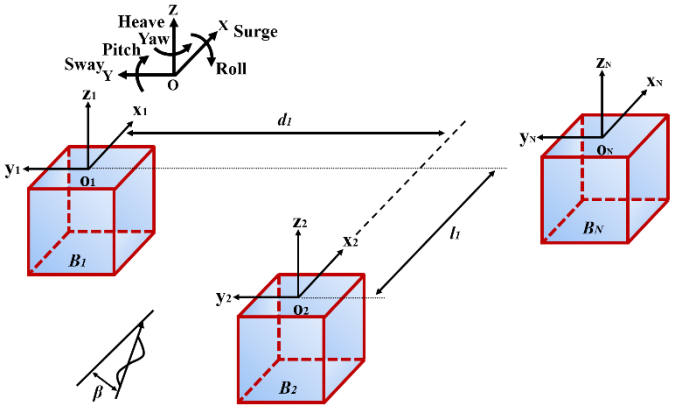

FIGURE 2: COORDINATE SYSTEMS.

Assuming the surrounding fluid is ideal, linear potential flow theory is used to model the hydrodynamic properties of large arrays of modularized FPV bases. The velocity potential which satisfies the Laplace equation is introduced to describe the whole fluid. The linearized velocity potential can be expressed by

$$\Psi(\vec{X},t) = Re\left[\eta_0\varphi_0(\vec{X})e^{-i\omega_0 t}\right] + Re\sum_{j=1}^{6}\sum_{m=1}^{N}\left[\eta_j^m\varphi_j^m(\vec{X})e^{-i\omega_0 t}\right] + Re\left[\eta_7\varphi_7(\vec{X})e^{-i\omega_0 t}\right] \quad (1)$$

where ω_0 is the frequency of incident wave; N is the total number of modularized floating bases in an FPV array; φ_0 is the unit incident potential and $\eta_0 = \eta_7$ is the incident wave amplitude; φ_j^m (j=1, 2, …, 6, m=1, 2, …, N) is the unit radiated wave potential in 6 degrees of freedom (DoF) and η_j^m is the corresponding oscillation amplitude; φ_7 is the unit diffracted wave potential.

The incident wave potential φ_0 can be written as

$$\varphi_0 = -\frac{ig\eta_0}{\omega_0}\frac{\cosh k(z+d)}{\cosh kd}e^{i[k(x\cos\beta + y\sin\beta)]} \quad (2)$$

in which d is the water depth; β is the incident wave angle; k is the wave number that satisfies the dispersion relation

$$k\cdot\tanh kd = {\omega_0}^2/g \quad (3)$$

The diffraction and radiation problems can be treated by solving the following governing equations and boundary conditions:

(1) Diffraction wave potential

$$\nabla^2\varphi_7 = 0 \quad \text{in the fluid domain;} \quad (4)$$

$$g\frac{\partial\varphi_7}{\partial z} - {\omega_0}^2\varphi_7 = 0 \quad \text{on the undisturbed free surface } S_f; \quad (5)$$

$$\frac{\partial\varphi_7}{\partial n} = -\frac{\partial\varphi_0}{\partial n}|_{S_m} \quad \text{on the mean wetted body surface } S_m; \quad (6)$$

$$\frac{\partial \varphi_7}{\partial z} = 0 \qquad \text{on the seabed.} \tag{7}$$

(2) Radiation wave potential

$$\nabla^2 \varphi_j^m = 0 \qquad \text{in the fluid domain;} \tag{8}$$

$$g\frac{\partial \varphi_j^m}{\partial z} - {\omega_0}^2 \varphi_j^m = 0 \qquad \text{on the undisturbed free surface } S_f; \tag{9}$$

$$\frac{\partial \varphi_j^m}{\partial n} = \begin{cases} -i\omega_0 n_j|_{S_m} \\ 0|_{S_{others}} \end{cases} \qquad \text{on the wetted body surface } S_m \ (B_m \text{ is oscillating while others are fixed}); \tag{10}$$

$$\frac{\partial \varphi_j^m}{\partial n} = 0 \qquad \text{on the seabed.} \tag{11}$$

After deriving the velocity potentials, the pressure on each FPV floater surface can be obtained from Bernoulli's equation:

$$p_j^m = -i\omega\rho\varphi_j^m, \qquad j = 0, 1, \dots, 6, 7;\ m = 1, 2, \dots, N \tag{12}$$

where ρ is the fluid density.

The wave excitation forces can then be obtained by integrating the incident and diffraction pressures as

$$F_i^{W_m} = \iint_{S_m} (p_0 + p_7)\, n_i dS \tag{13}$$

Furthermore, the hydrodynamic forces produced by the oscillatory motions of the body in 6 DoF can be obtained from the radiation potentials as

$$\begin{aligned} F_i^{R_m} &= \sum_{j=1}^{6} \iint_{S_m} p_j^m\, n_i dS \cdot \left(\sum_{n=1}^{N} \eta_j^n\right) \\ &= \sum_{j=1}^{6}\sum_{n=1}^{N} \left(\omega_0^2 \mu_{ij}^{mn} + i\omega_0 \lambda_{ij}^{mn}\right)\eta_j^n,\ i = 1, 2, \dots, 6; m = 1, 2, \dots, N \end{aligned} \tag{14}$$

where μ_{ij}^{mn} is the added mass coefficient of the m-*th* body in the i_{th} mode which is induced by the oscillation motion of the n-*th* body in the j_{th} mode; λ_{ij}^{mn} is the damping coefficient in which the definitions of subscript and superscript are the same as those of added mass. The added mass and damping coefficients can be obtained by

$$\mu_{ij}^{mn} = -\frac{\rho}{\omega_0}\iint_{S_m} \varphi_{Ij}^n\, n_i dS, \qquad i, j = 1, 2, \dots, 6;\ m, n = 1, 2, \dots, N \tag{15}$$

$$\lambda_{ij}^{mn} = -\rho \iint_{S_m} \varphi_{Rj}^n\, n_i dS, \qquad i, j = 1, 2, \dots, 6;\ m, n = 1, 2, \dots, N \tag{16}$$

Once the unknown wave excitation forces and radiation hydrodynamic coefficients are solved, the dynamic equation of motion for the interconnected floating structures in the frequency domain can be written as

$$\begin{bmatrix} -\omega_0^2(\boldsymbol{M}+\boldsymbol{\mu}) + i\omega_0(\boldsymbol{\lambda}+\boldsymbol{C_d}) + (\boldsymbol{K}+\boldsymbol{K_s}) & \boldsymbol{D}_J^T \\ \boldsymbol{D}_J & \boldsymbol{0} \end{bmatrix} \begin{Bmatrix} \boldsymbol{\eta} \\ \boldsymbol{F}_J \end{Bmatrix} = \begin{Bmatrix} \boldsymbol{F}^W \\ \boldsymbol{0} \end{Bmatrix} \tag{17}$$

where $\boldsymbol{M}$ and $\boldsymbol{K}$ are the mass and stiffness matrix of $(6N \times 6N)$, in which N is the total number of floating structures; $\boldsymbol{\mu}$ and $\boldsymbol{\lambda}$ are added mass and potential damping matrix of $(6N \times 6N)$; $\boldsymbol{C_d}$ is the damping matrix of the damper installed between adjacent floaters; $\boldsymbol{K_s}$ is the stiffness matrix of the spring installed between adjacent floaters; $\boldsymbol{D}_J$ is the displace constraint matrix of $(M \times 6N)$, in which M represents the number of joint constraints [5]; $\boldsymbol{\eta}$ is the frequency-dependent displacements array of $(6N \times 1)$; $\boldsymbol{F}_J$ is the joint force vector of $(M \times 1)$; $\boldsymbol{F}^W$ is the wave excitation force array of $(6N \times 1)$.

If the bodies are oscillating independently, the body motions in frequency domain Eq. (17) can be simplified as

$$[-\omega_0^2(\boldsymbol{M}+\boldsymbol{\mu}) + i\omega_0\boldsymbol{\lambda} + \boldsymbol{K}]\{\boldsymbol{\eta}\} = \{\boldsymbol{F}^W\} \tag{18}$$

2.2 Interaction cut-off scheme for modularized FPV arrays

FPV arrays are usually composed of hundreds of individual floaters, which have identical body shapes and are systematically arranged on the ocean surface. It requires significant computational resources to resolve the hydrodynamic interactions among these modularized floaters, especially the radiation interactions. To save the computational cost, a numerical scheme is developed to improve the efficiency of radiation calculations by neglecting the coupling terms when the distance between the m- and n-*th* body is sufficiently large. In the proposed hydrodynamic modelling scheme, *N* cut-off circles are defined with each floater as the individual circle centre and the same truncation distance as the radius. If the n-*th* floater is located outside the defined cut-off circle with the circle centre fixed on the m-*th* body, the coupling terms φ_j^{mn} will be ignored. Obviously, a smaller radius is desired for fast computations. However, it may be accompanied by worse results accuracy. The radius of the cut-off circle is determined by a few parameters, including the body shape, the wave frequency, and the accuracy requirement. To balance the computational accuracy and efficiency, an optimal cut-off radius associated with the truncation error *Et* should be quantified.

A 15-floater FPV array, shown in Figure 3, is chosen to explain why the developed cut-off scheme could be used to save computational time. Figure 4 shows the radiation interaction matrix of the 15-body array. Obviously, the interaction matrix will be sparse when the cut-off circle is introduced. Theoretically, each body can oscillate independently in 6 DoFs. The total unknown element number of the full radiation interaction matrix is 6×15^2, indicating we have to solve the coupling terms φ_j^{mn} 1,350 times independently to obtain the radiation hydrodynamic properties of the array. However, if the distance between the m- and n-*th* floater is greater than the defined cut-off radius *R*, the coefficient located in the m-*th* row, n-*th* column of the radiation interaction matrix will be assumed to be 0. Therefore, the unknown element number is reduced to

6×78. It explains how the computational cost is reduced. It can be imagined that when the size of the array increases, more computational time can be saved, which enables feasible modelling of the hydrodynamic properties of large FPV arrays.

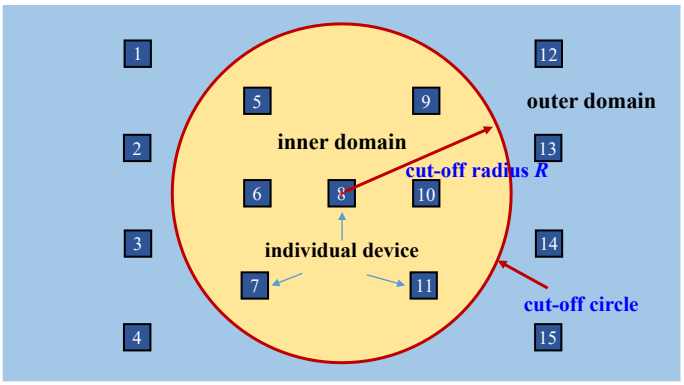

FIGURE 3: AN EXAMPLE OF THE CUT-OFF SCHEME FOR MODULARIZED FPV ARRAYS.

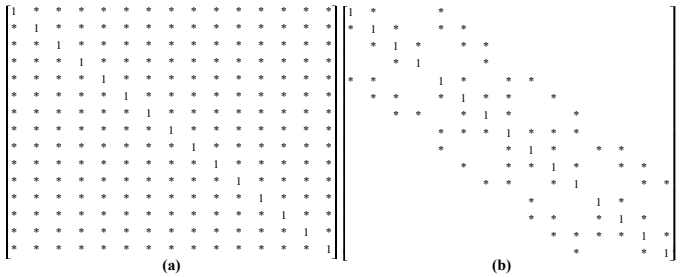

FIGURE 4: RADIATION INTERACTION MATRIX OF A 15-FLOATER FPV ARRAY. (a) FULL RANK MATRIX CONSIDERING INTERACTIONS AMONG ALL DEVICES; (b) SPARSE MATRIX INTRODUCING CUT-OFF RADIUS.

3. RESULTS AND DISCUSSIONS

As we have discussed in Section 2, the cut-off radius R is a crucial parameter to balance the results accuracy and computational time. The three-dimensional boundary element programme MHydro, used in Yuan *et al*. [17], will be applied to quantify the optimal R and to perform the proposed cut-off scheme in the present study.

3.1 Optimal cut-off radius diagram

To find the optimal cut-off radius R, it requires extensive numerical simulations of 2-body arrays with the identical body shape but different separation distances. The details of how to quantify the radiation interaction effects can be found in Zhang *et al*. [16]. In the present study, the same square boxes with a diameter of L=1 m as in Zhang *et al*. [16] are chosen as the floaters for the FPV arrays in the present study. Taking truncation errors of 5%, 15%, 30%, and 50% as examples, the critical curves associated with truncation error, wave frequency, and separation distance can be described and shown in Figure 5. The distance-frequency plane can be divided into two domains by each critical curve: lower-left domain and upper-right domain. When the combination of wave frequency and separation distance is located in the lower-left domain, the radiation interactions between the m- and n-*th* bodies have to be calculated. As the truncation error *Et* increases, the scope of the upper-right domain gradually expands. It indicates that the proposed cut-off scheme can be implemented over a wider frequency range to save more time when a larger *Et* is chosen. Furthermore, a clear downward trend of the critical curves can be found, which indicates that the oscillation of one body could hardly influence the hydrodynamic properties of another floating body.

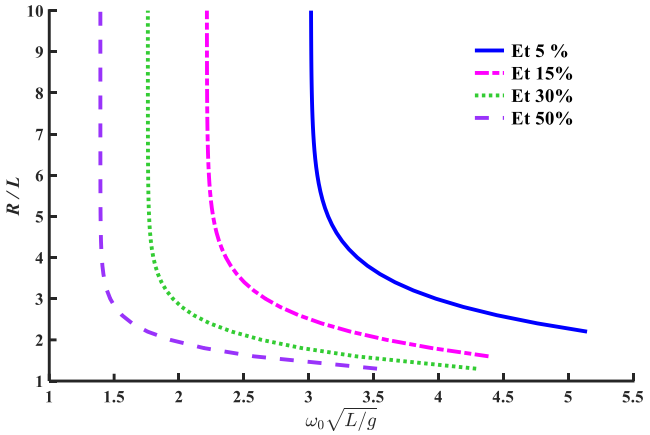

FIGURE 5: CRITICAL CURVES SHOWING WHETHER THE HYDRODYNAMIC INTERACTION EFFECTS CAN BE IGNORED.

3.2 Effect of wave direction

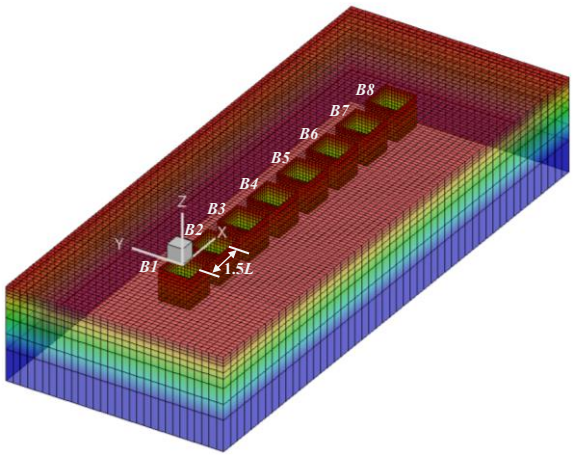

FIGURE 6: PANEL DISTRIBUTION OF THE NUMERICAL MODELS FOR A COLUMN OF FPV ARRAY AT 0.5L GAP DISTANCE.

The present cut-off scheme makes it feasible to balance the results accuracy and computational time when modelling the hydrodynamic properties of the modularized floaters in an FPV array. A column of FPV floaters is chosen here to examine the results accuracy and computational efficiency of the developed FPV hydrodynamic modelling method. The floaters layout and computational domain are shown in Figure 6. The gap distance between adjacent floaters is 0.5L. The range of incident

wavelength is given as $\lambda/L = 0 - 5$. The performance of an FPV array is mainly determined by the relative angle between the solar panels and sunlight. Therefore, only pitch motions are compared in this section.

To examine the results accuracy and computational efficiency of the developed cut-off scheme, two parameters defined in Zhang *et al.* [16], i.e. the relative errors *Er* and the time consumption ratio *Ct*, are also applied in the present study. A smaller *Er* donates a more accurate result. Similarly, a smaller *Ct* means a shorter computational time is needed. Figure 7 shows the relative errors of the 8-floater FPV array at wave direction $\beta = 0^{\circ}$. It can be clearly observed that a smaller *Et* is always accompanied by a higher computational accuracy. Even if *Et*=50% is chosen, the pitch motion is well predicted with *Er* not exceeding 8%. This is due to the fact that the motion responses are not only determined by the radiation coefficients. In most of the frequency range, the mass, restoring matrix, and excitation forces have a more dominant influence. Meanwhile, between *Et*=15% and *Et*=30%, a very noticeable difference in *Er* can be found. This can be explained by Figure 5. At *Et*=5% or 15%, the minimum cut-off radius is 2.2*L* and 1.6*L* respectively, where the radiation interactions between adjacent floaters are still considered at large wave frequencies. However, these interactions are ignored at *Et*=30% and 50%.

The relative errors for each floater are summed and then averaged to show the effect of different incident wave directions on the proposed scheme. The average relative errors Er_{av} and time consumption ratio *Ct* are summarized in Table 1. *Et* =0% means that the full hydrodynamic interactions are considered in the calculations. For any given wave direction, the motion responses can be well predicted, and the computational times are all less than 50% of the simulations with full consideration of the radiation interactions.

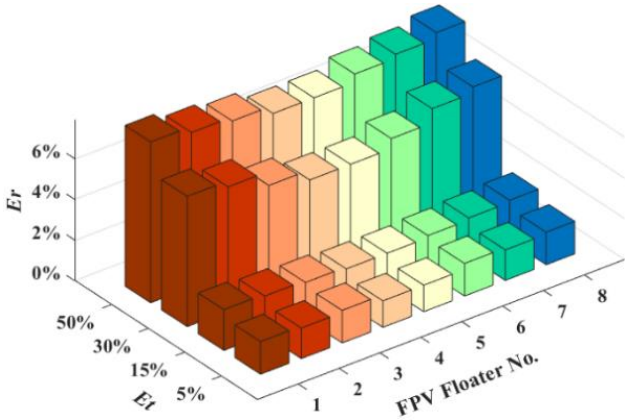

FIGURE 7: RELATIVE ERRORS OF PITCH MOTION AT WAVE DIRECTION $\beta = 0^{\circ}$.

TABLE 1: AVERAGE RELATIVE ERRORS (%) AND TIME CONSUMPTION RATIO AT DIFFERENT WAVE DIRECTIONS.

	Wave direction				*Ct*
Et	0	$\pi/6$	$\pi/4$	$\pi/3$	
0%	0	0	0	0	1
5%	1.50	1.37	1.39	1.48	0.43
15%	1.85	1.87	1.81	1.77	0.39
30%	5.70	5.93	5.73	5.85	0.33
50%	7.47	7.44	7.46	7.63	0.31

3.3 Effect of gap distance

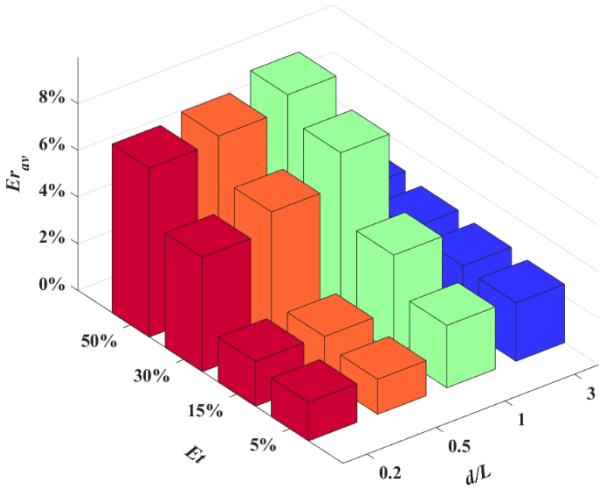

FIGURE 8: AVERAGE RELATIVE ERRORS OF PITCH MOTION AT DIFFERENT GAP DISTANCE.

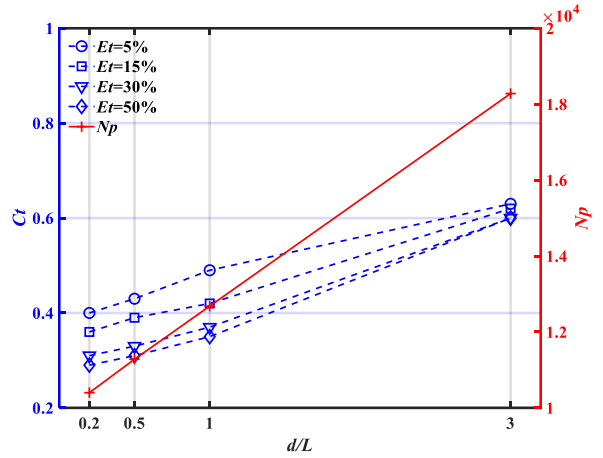

FIGURE 9: TIME CONSUMPTION RATIO AND TOTAL PANEL NUMBER AT DIFFERENT GAP DISTANCES.

Figure 8 shows the average relative errors associated with different gap distances between the adjacent FPV floaters. As the truncation errors *Et* increase, the average relative errors basically show an upward trend. This is consistent with the conclusion described in Subsection 3.1. The effect of gap distance on the results accuracy can also be found in Figure 8. Four cases with different gap distances are designed here. Obviously, at *d*/*L*=3, the average relative errors Er_{av} corresponding to the different *Et* are relatively small. This is due to the fact that when the distance between the floaters is large enough, the hydrodynamic interaction between them will be slight. So, even though all four minimum cut-off radii are smaller than the distance between adjacent floaters at *d*/*L*=3, this would not result in a significant impact on the accuracy of the motion results. The differences among these four Er_{av} arise mainly from the different starting

wave frequencies at which the cut-off scheme is introduced. However, at the other three gap distances, the results errors corresponding to the different *Et* are more varied. At *d*/*L*=1, the minimum cut-off radius will be smaller than the distance between the adjacent floaters when Et>5%, so there is a more significant variation between *Et*=5% and *Et*=15%. However, at *d*/*L*=0.5 or *d*/*L*=0.8, the minimum cut-off radius will be smaller than the distance between the adjacent floaters only at *Et*>30%. This explains why the *Et* corresponding to the significant growth change in Er_{av} is different for various gap distances. Generally, the effect of gap distance on the results accuracy depends mainly on whether the distance between the adjacent floaters is lower than the minimum cut-off radius.

Figure 9 shows the time consumption ratio *Ct* and total panel number *Np* in the entire computational domain. As the gap distance increases, the proposed method takes more time to predict the motion responses of the FPV array. The ratio of panel number on each body surface to the total panel number can explain this increasing trend. When the gap distance becomes larger, the proportion of panels which can be ignored becomes smaller because the entire computational domain has more computational panels.

3.4 Effect of connection types

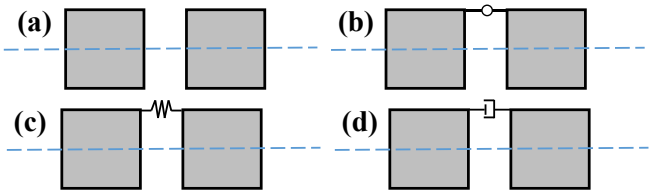

FIGURE 10: SKETCH OF FOUR CONNECTION TYPES. (a) INDEPENDENT MOTION; (b) HINGE CONNECTION; (c) SPRING CONNECTION; (d) DAMPER CONNECTION.

To investigate the effect of connector on the developed method, a series of cases are designed based on four different connection types: independent oscillation (C1), hinge-type connection (C2), spring-type connection (C3), and damper-type connection (C4). Figure 10 is the side view of these connection types. In these cases, the wave direction is 0° and the gap distance is 0.5*L*. The average relative errors Er_{av} and time consumption ratio *Ct* of the pitch motions with different connectors are presented in Figure 11 and Figure 12 respectively. Two stiffness and damping coefficients are applied to spring-type and damper-type connections respectively. The stiffness and damping coefficients are expressed in the following dimensionless terms:

$$Ks = \frac{k_{spring}}{\rho g V L} \tag{19}$$

$$Cd = \frac{c_{damper}\sqrt{gd}}{\rho g V L^2} \tag{20}$$

where *V* is the volume of an FPV floater; *L* is the floater length; *d* is the water depth.

From the results of Figure 11, it can be clearly observed that there is no significant difference in the average relative errors across various case studies with different connection types. It indicates that the connection types have no noticeable effect on the accuracy of the motion responses predicted by the developed cut-off scheme. Furthermore, the values of average relative errors are small for each case, it suggests that the motion response of FPV arrays with different connectors can be well predicted by the proposed method. From Figure 12, we can find four time-consumption-ratio curves are straight lines and all below 0.5 from *Et*=5% onwards. It indicates that the proposed cut-off scheme is effective in saving computational time and shows that solving for the motion responses of FPV arrays with different connectors has no influence on the computational efficiency of the developed method.

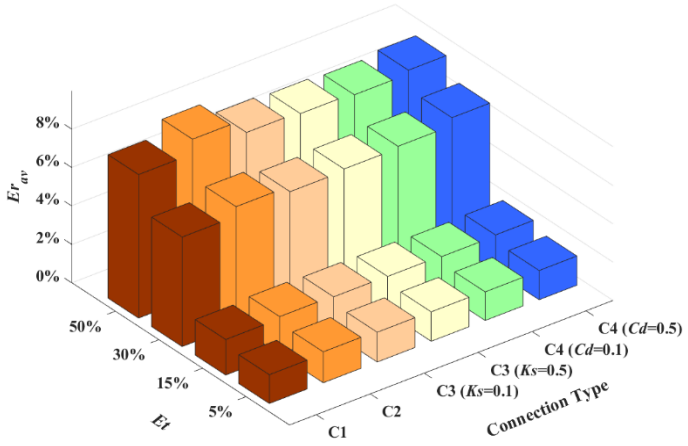

FIGURE 11: AVERAGE RELATIVE ERRORS OF PITCH MOTION WITH DIFFERENT CONNECTION TYPES.

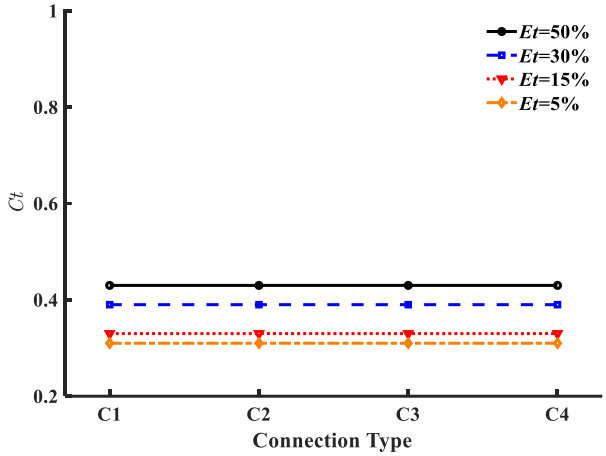

FIGURE 12: TIME CONSUMPTION RATIO WITH DIFFERENT CONNECTION TYPES.

4. CONCLUSION

This study proposes a radiation interactions cut-off scheme, which can be implemented in the multi-body hydrodynamic solvers to save the computational time when modelling large arrays of modularized FPV floaters. Based on the numerical

simulations of an FPV array, the accuracy and efficiency of the developed cut-off scheme are examined. From the investigated above, the following conclusions can be drawn:

1) For any given wave frequency and truncation error, an optimal cut-off radius can always be determined. Based on the simulations of the 2-body array, some critical curves can be obtained, which can be used to determine whether the hydrodynamic interactions can be ignored.

2) The motion responses of FPV floaters can be well predicted by the developed cut-off scheme, even if Et=50% is applied. Meanwhile, the proposed method can significantly improve the computational efficiency to predict the motion responses of FPV arrays.

3) Wave direction and connection type have a weak influence on the accuracy and efficiency of the proposed scheme. As the total number of panels in the entire computational domain increases, the computational time saved by the developed method decreases accordingly.

ACKNOWLEDGEMENTS

The present work is supported by the National Natural Science Foundation of China (No. 52088102 and No. 51979131). The first author De-Qing Zhang is also supported by the China Scholarship Council.

REFERENCES

[1] Ranjbaran, P., Yousefi, H., Gharehpetian, G. B., Astaraei, F. R., 2019. A review on floating photovoltaic (FPV) power generation units. Renewable and Sustainable Energy Reviews, 110(2019), 332-347.

[2] Sahu, A., Yadav, N., Sudhakar, K., 2016. Floating photovoltaic power plant: A review. Renewable and Sustainable Energy Reviews, 66(2016), 815-824.

[3] Vo, T. T. E., Ko, H., Huh, J., Park, N., 2021. Overview of possibilities of solar floating photovoltaic systems in the offshore industry. Energies, 14(21), 6988.

[4] López, M., Rodríguez, N., Iglesias, G., 2020. Combined floating offshore wind and solar PV. Journal of Marine Science and Engineering, 8(8), 576.

[5] Zheng, S., Zhang, Y., 2017. Analysis for wave power capture capacity of two interconnected floats in regular waves. Journal of Fluids and Structures, 75, 158-173.

[6] Liang, H., Chua, K. H., Wang, H. C., Choo, Y. S., 2021. Numerical and experimental investigations into fluid resonance in a gap between two side-by-side vessels. Applied Ocean Research, 111, 102581.

[7] Jin, S., Wang, D., Hann, M., Collins, K., Conley, D., Greaves, D., 2023. A designed two-body hinged raft wave energy converter: from experimental study to annual power prediction for the EMEC site using WEC-Sim. Ocean Engineering, 267, 113286.

[8] Borgarino, B., Babarit, A., Ferrant, P., 2012. Impact of wave interactions effects on energy absorption in large arrays of wave energy converters. Ocean Engineering, 41, 79-88.

[9] Engström, J., Eriksson, M., Göteman, M., Isberg, J., Leijon, M., 2013. Performance of large arrays of point absorbing direct-driven wave energy converters. Journal of Applied Physics, 114, 204502.

[10] Teng, B., Gou, Y., 2006. Fast multipole expansion method and its application in BEM for wave diffraction and radiation, Proceedings of the 16th International Offshore and Polar Engineering Conference. pp. 318-325.

[11] Borgarino, B., Babarit, A., Ferrant, P., 2012. An implementation of the fast multipole algorithm for wave interaction problems on sparse arrays of floating bodies. Journal of Engineering Mathematics, 77(1), 51-68.

[12] Singh, J., Babarit, A., 2014. A fast approach coupling Boundary Element Method and plane wave approximation for wave interaction analysis in sparse arrays of wave energy converters. Ocean Engineering, 85, 12-20.

[13] Budal, K., 1977. Theory for absorption of wave power by a system of interacting bodies. Journal of Ship Research, 21(04), 248-254.

[14] Fitzgerald, C., Thomas, G., 2007. A preliminary study of the optimal formation of an array of wave power devices, Proceedings of the 7th European Wave and Tidal Energy Conference, Porto, Portugal.

[15] Göteman, M., Engström, J., Eriksson, M., Isberg, J., 2015. Fast Modeling of Large Wave Energy Farms Using Interaction Distance Cut-Off. Energies, 8(12), 13741-13757.

[16] Zhang, D., Yuan, Z. M., Du, J., Li, H., 2022. Hydrodynamic modelling of large arrays of modularized floating structures with independent oscillations. Applied Ocean Research, 129, 103371.

[17] Yuan, Z.-M., Ji, C.-Y., Incecik, A., Zhao, W., Day, A., 2016. Theoretical and numerical estimation of ship-to-ship hydrodynamic interaction effects. Ocean Engineering, 121, 239-253.